Article

Heterogeneous Gold Nanoparticle-Based Catalysts for the Synthesis of Click-Derived Triazoles via the Azide-Alkyne Cycloaddition Reaction

Ivy L. Librando [1], Abdallah G. Mahmoud [1,2], Sónia A. C. Carabineiro [1,3,4,*], M. Fátima C. Guedes da Silva [1], Francisco J. Maldonado-Hódar [5], Carlos F. G. C. Geraldes [6,7] and Armando J. L. Pombeiro [1,8]

[1] Centro de Química Estrutural, Instituto Superior Técnico, Universidade de Lisboa, Av. Rovisco Pais, 1049-001 Lisboa, Portugal; ivy.librando@tecnico.ulisboa.pt (I.L.L.); abdabdallah.mahmoud@tecnico.ulisboa.pt (A.G.M.); fatima.guedes@tecnico.ulisboa.pt (M.F.C.G.d.S.); pombeiro@tecnico.ulisboa.pt (A.J.L.P.)
[2] Department of Chemistry, Faculty of Science, Helwan University, Ain Helwan, Cairo 11795, Egypt
[3] Laboratory of Catalysis and Materials (LCM), Associate Laboratory LSRE-LCM, Faculty of Engineering, University of Porto, 4200-465 Porto, Portugal
[4] LAQV-REQUIMTE, Department of Chemistry, NOVA School of Science and Technology, Universidade NOVA de Lisboa, 2829-516 Caparica, Portugal
[5] Department of Inorganic Chemistry, Faculty of Sciences, University of Granada, Avenida de Fuente Nueva, s/n, 18071 Granada, Spain; fjmaldon@ugr.es
[6] Department of Life Sciences, Faculty of Science and Technology, Calçada Martim de Freitas, 3000-393 Coimbra, Portugal; geraldes@uc.pt
[7] Coimbra Chemistry Center, University of Coimbra, Rua Larga Largo D. Dinis, 3004-535 Coimbra, Portugal
[8] Research Institute of Chemistry, Peoples' Friendship University of Russia (RUDN University), 6 Miklukho-Maklaya Street, 117198 Moscow, Russia
* Correspondence: sonia.carabineiro@fct.unl.pt

Abstract: A supported gold nanoparticle-catalyzed strategy has been utilized to promote a click chemistry reaction for the synthesis of 1,2,3-triazoles via the azide-alkyne cycloaddition (AAC) reaction. While the advent of effective non-copper catalysts (i.e., Ru, Ag, Ir) has demonstrated the catalysis of the AAC reaction, additional robust catalytic systems complementary to the copper catalyzed AAC remain in high demand. Herein, Au nanoparticles supported on Al_2O_3, Fe_2O_3, TiO_2 and ZnO, along with gold reference catalysts (gold on carbon and gold on titania supplied by the World Gold Council) were used as catalysts for the AAC reaction. The supported Au nanoparticles with metal loadings of 0.7–1.6% (*w/w* relative to support) were able to selectively obtain 1,4-disubstituted-1,2,3-triazoles in moderate yields up to 79% after 15 min, under microwave irradiation at 150 °C using a 0.5–1.0 mol% catalyst loading through a one-pot three-component (terminal alkyne, organohalide and sodium azide) procedure according to the "click" rules. Among the supported Au catalysts, Au/TiO_2 gave the best results.

Keywords: Au nanoparticles; supported catalysts; azide-alkyne; 1,2,3-triazoles

1. Introduction

Interest in metal nanoparticle-based catalysis is strongly increasing as a stable and competitive alternative to conventional catalysis [1]. Numerous efforts have been made to synthesize metal nanoparticles with controllable size and morphology which is pivotal in determining their catalytic properties [2], The catalytic use of nanostructured materials suspended in colloidal solutions, as well as those deposited on different supports for organic transformations, were highlighted in many studies [3–5]. While uniform nanoparticle suspensions are considered as the bridge between traditional homogenous and heterogeneous catalysis [6], metal nanoparticles have gained considerable attention due to their unique properties and extremely large surface-to-volume ratio which differ greatly from their

corresponding bulk substances [7]. Since the discovery that gold metal species can act as a catalysts [8,9], gold nanoparticles (Au NPs) have emerged as key materials in nanoscience and have been intensively studied ever since [10–13]. Heterogeneous Au catalysts have applications in many reactions of industrial and ecological relevance [5,14,15]. They are considered as one of the most powerful activators of C-C multiple bonds, which allows the formation of C-C, C-O, C-N, and C-S bonds by nucleophilic attack on the reactive multiple bonds [16,17]. Consequently, their catalytic activity is significantly impacted by the preparation method, the nature of the support, and in particular, the size and shape of the nanoparticles [5,15].

While many reactions performed with gold catalysts have been reported, the Au-catalyzed alkyne-azide cycloadditions (AuAAC), leading to 1,4- and 1,5-disubstituted-1,2,3-triazoles, have remained elusive [4,18,19]. The 1,2,3-triazoles are prominent nitrogen-containing heterocyclic motifs that have widespread applications in areas ranging from medicinal chemistry to materials science [20–23]. Although elegant preparative methods for such motifs have been reported [24–30], versatile and practical methodologies for the synthesis of substituted 1,2,3-triazoles beyond the use of copper-based catalysts are still desirable. Despite the advent of effective non-copper catalysts (i.e., Ru, Ag, Ir) [31,32] which have also demonstrated to catalyze the azide-alkyne cycloaddition (AAC) reaction, additional robust catalytic systems that can provide complementary selectivity or relative reactivity to the copper catalyzed AAC remain in high demand.

In the past years, copper catalysts have played an important role in azide-alkyne cycloadditions [33,34], and the CuAAC reaction found applications in various scientific fields [35–37]. Despite the great advantages of CuAAC, there remains some drawbacks, such as the need of oxidative or reductive agents and a significant amount of catalyst is required. As Cu(I) salts are quite prone to redox processes, phosphorus- or nitrogen-based ligands are usually required to protect and stabilize the active Cu catalyst during the cycloaddition reaction. These problems and the wide applicability of this reaction have led the scientific community to explore the possibility of an attractive click-compatible heterogeneous version.

In 2013, Muthusubramanian et al. [4] reported the use of titania-supported Au NPs as catalyst for the Huisgen [3 + 2] cycloaddition of azides and alkynes following a stepwise reaction pathway. The studied Au catalysts were able to produce the 1,4-disubstiuted-1,2,3-triazoles in good to excellent yields. In the following year, Huang et al. [18] studied the ability of gold nanocubes, octahedra and rhombic dodecahedra to catalyze AAC reactions where several triazoles were obtained from a variety of alkynes and organic azides in good yields using the smallest gold rhombic-dodecahedral nanocrystals in the presence of triethylamine base.

In association with our research interest on the development of effective catalysts for the AAC reaction, this current study presents the use of Au NPs supported on various metal oxides (viz., Al_2O_3, Fe_2O_3, TiO_2 and ZnO) as heterogenous catalysts. In contrast to the previous stepwise methodologies for AuAAC [4,18] that involved using the unfavourable organic azides, herein a one-pot, three-component protocol was studied under microwave irradiation (MW) where the organic azides are formed in situ by reacting organohalide with sodium azide (Scheme 1). The present method also showcased a ligand-, oxidant/reductant- and additive-free AAC with a short reaction time as compared to the previously reported copper-based [28,38,39] cycloaddition reactions.
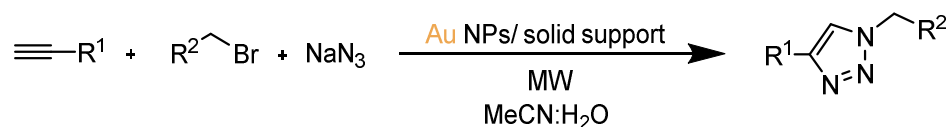

Scheme 1. Synthesis of triazoles catalyzed by Au nanoparticles on different metal oxide supports under MW irradiation.

2. Results and Discussion

2.1. Synthesis and Characterisation of Supported Au NPs

Au NPs supported on different commercial metal oxides, namely Al_2O_3, Fe_2O_3, TiO_2 and ZnO, were obtained via deposition-precipitation method. The prepared gold catalysts as well as gold reference catalysts, supplied by the World Gold Council (W) [40], namely gold on carbon (Au/C Gold Catalyst Type D) and gold on titania (Au/TiO_2 Type A), were characterized.

The morphology of the oxide supports was analysed by SEM (scanning electron microscopy), as shown in Figure 1. The SEM images showed that alumina (Figure 1a) had a homogeneous cloudy appearance while Fe_2O_3 had a somewhat "coral skeleton" porous structure (Figure 1b). The TiO_2 support produced an image of homogeneous agglomerates (Figure 1c) and ZnO showed a mixture of particle agglomerates while some parts had a resemblance of thin veils (Figure 1d).
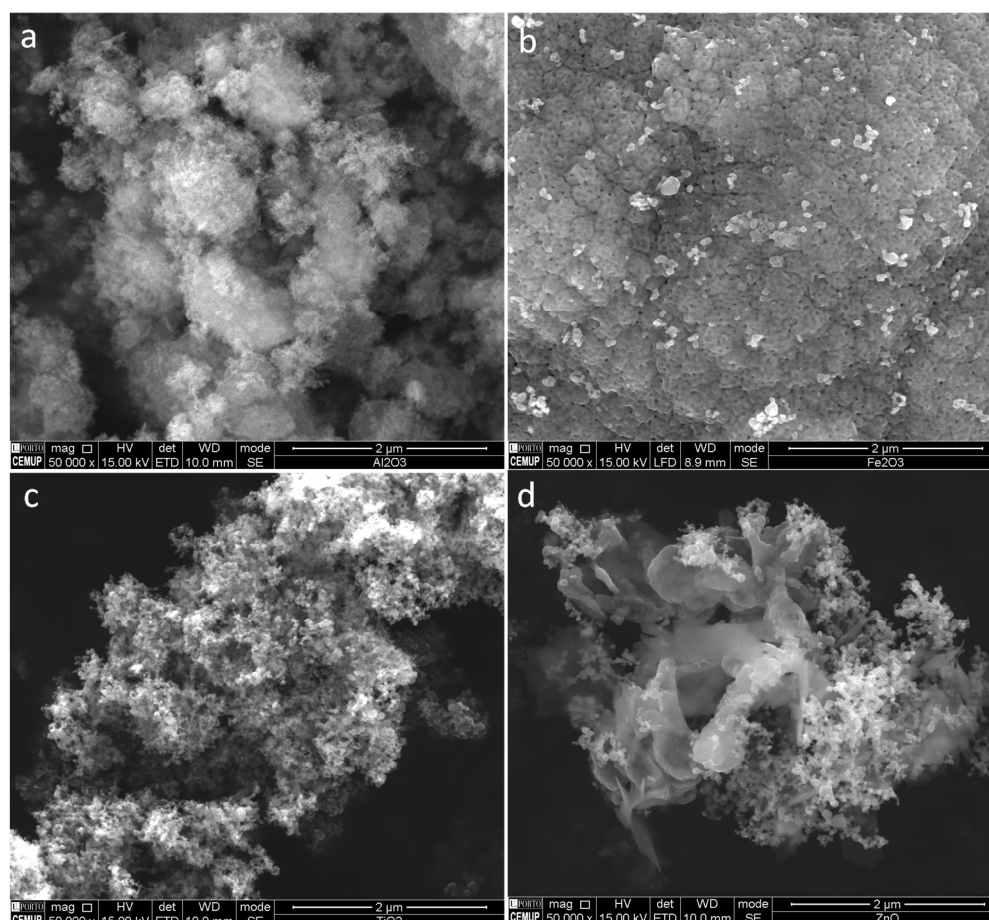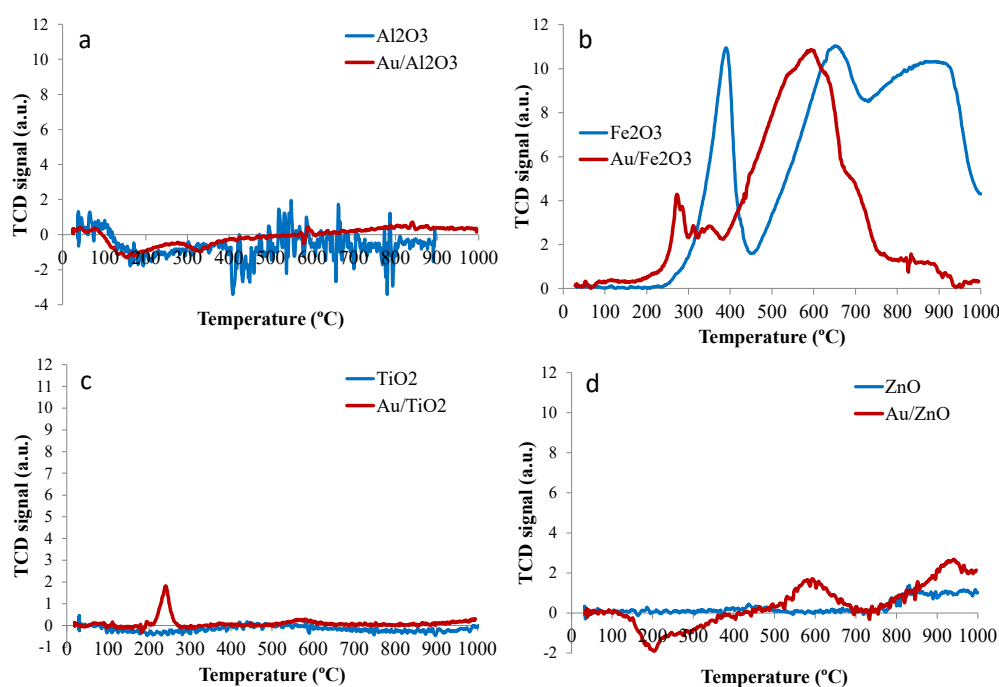

Figure 1. The SEM images of supports: (**a**) Al_2O_3, (**b**) Fe_2O_3, (**c**) TiO_2, (**d**) ZnO.

Table 1 shows the comparison of Brunauer-Emmett-Teller (BET) surface area (S_{BET}) of the supports before and after the immobilization of Au. The BET surface area of the oxides was generally low and remained unaffected by the addition of Au, most probably due to the low metal loading and small particle size of Au. From the samples being studied, alumina (210 m^2/g) had the highest surface area, while Fe_2O_3 showed the lowest value of 5 m^2/g. Both TiO_2 (51 m^2/g) and ZnO (26 m^2/g) supports exhibited intermediate values. In terms of total pore volume (measured at $P/P_o = 0.99$), alumina showed the largest size (1.24 cm^3 g^{-1}), followed by Fe_2O_3 (0.62 cm^3 g^{-1}), TiO_2 (0.25 cm^3 g^{-1}) and ZnO (0.08 cm^3 g^{-1}), as shown in Table 1. Concerning pore size, measured by the Barrett-Joyner-Halenda (BJH) desorption method, alumina showed the largest value (19.6 nm), followed by ZnO (12.5 nm), while Fe_2O_3 and TiO_2 showed similar values (3.1 and 3.4 nm,

respectively), as also displayed in Table 1. Supplementary Figure S1 shows the isotherms and pore size distributions of these metal oxides. It can be seen that the materials present isotherms characteristics of materials with weak interaction and hysteresis typical of slit shaped pores. The pore size distributions show that the majority of pores have radius below 100 Å.

The XRD (X-ray diffraction) results of the supports and gold containing samples are also given in Table 1. Au was not detected due to the low loading content and small nanoparticle size range. As for the supports, Al_2O_3 gave a mixture of γ- and θ-alumina; Fe_2O_3 showed a hematite crystal structure; TiO_2 (P25) showed a mixture of anatase (80%) and rutile (20%); while ZnO was detected on this oxide.

Figure 2 shows the superimposed temperature-programmed reduction (TPR) profiles of the supports and the gold containing samples and temperature of the main peaks are summarized in Table 1. The Al_2O_3 profile (Figure 2a) did not show any significant reduction peaks, as expected for an irreducible oxide [5,41], while Fe_2O_3 (Figure 2b) showed several reduction peaks, such as the peak at 391 °C that can be attributed to the reduction of hematite to magnetite (Fe_3O_4) [5,42,43] the peak at 660 °C that represents the reduction of Fe_3O_4 to wustite (FeO) [5,44,45] and the peak >800 °C that is attributed to the reduction of FeO to Fe [46,47]. In the Au/Fe_2O_3 sample, as Au is in the Au^+ state, a sharp peak was observed at 272 °C and can be assigned to the Au reduction (Au^0) [45,48]. The TiO_2 support does not show any significant reduction peaks (Figure 2c) [5,49], while the Au/TiO_2 sample shows a sharp peak at ~240 °C due to the reduction of Au ions [50]. The ZnO support shows a small peak above 800 °C (Figure 2d) [5,51] while the presence of Au creates a peak at 600 °C and the previous peak at 800–900 °C increases in intensity. A negative peak at ~200 °C is also observed, which is probably due to the result of the dehydroxylation process of ZnO [5,52] when $Zn(OH)_2$ was formed upon Au addition.


Figure 2. TPR profiles of supports and Au samples: (**a**) Al_2O_3, (**b**) Fe_2O_3, (**c**) TiO_2, (**d**) ZnO. Adapted from [5] with permission from Wiley.

X-ray photoelectron spectroscopy (XPS) was also performed on the supported Au samples. As shown in Figure 3, Au is in the metallic state on Al_2O_3 and ZnO, while it is in the Au^+ state on both Fe_2O_3 and TiO_2 supports. For Au 4f XPS spectra of Au/ZnO, there is a superimposition of the Zn 3p peak, which makes determination somehow uncertain. However, XPS spectra of Au 4d confirmed the presence of metallic gold.

Table 1. Characterization of oxide supports by N_2 adsorption at $-196\,^\circ C$, phases detected by XRD, temperatures of TPR peaks.

Sample	S_{BET}, $m^2\,g^{-1}$ [a]	Total Pore Volume, $cm^3\,g^{-1}$	Pore Size, nm	Phase Detected [b]	TPR Peaks, $^\circ C$ [a]
Al_2O_3	210	1.24	19.6	θ alumina; γ-alumina	**530**, 550 *
Au/Al_2O_3	210	n.d	n.d	n.d	**500**, 810 *
Fe_2O_3	6	0.62	3.1	hematite, α-Fe_2O_3	**245**, 391, 660, 896
Au/Fe_2O_3	5	n.d	n.d	hematite, α-Fe_2O_3; gold not detected	**75**, 274, 350, 599, 701, 879
TiO_2	51	0.25	3.4	Anatase (80%), rutile (20%)	**400**, 438 *
Au/TiO_2	49	n.d	n.d	n.d	**168**, 240, 371 *, 575 *
ZnO	26	0.08	12.5	ZnO	**376**, 436 *, 827
Au/ZnO	25	n.d	n.d	n.d	**452**, 595, 941

[a] Data from [5]; onset (bold) and peak maxima (plain text); * minimal peaks. [b] XRD data from [53–55]. n.d.—Not determined.
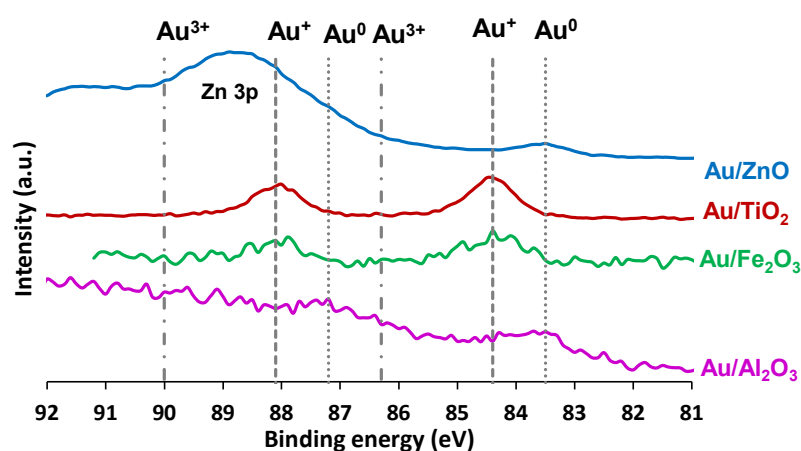
Figure 3. Au 4f XPS spectra of the supported Au nanoparticles on different supports. Adapted from [5] with permission from Wiley.

The supported Au nanoparticle samples were subjected to high-resolution transmission electron microscopy (HRTEM), shown in Figure 4, and results are summarized in Table 2. Au loaded on alumina shows a wide particle size distribution of 1–20 nm with average particle size of 3.6 nm (Figure 4a,b). Results for Au on Fe_2O_3 (Figure 4c,d) and TiO_2 (Figure 4e,f) were found to be of similar values, 2.3 nm and 2.2 nm, respectively (Table 2). Au/TiO_2 supplied by the World Gold Council (Au/TiO_2 W) showed a higher value of 3.7 nm, as determined by the supplier. Au on ZnO (Figure 4g,h) shows a smaller size range of 1–10 nm but gave an average particle size of 5.5 nm. Au/Fe_2O_3, on the other hand, had the smallest range of 1–7 nm while Au/TiO_2 gave the second largest range of 1–12 nm. Gold on carbon from the World Gold Council (Au/C W) showed a higher value of 10.5 nm, as informed by the supplier. The calculated Au dispersion (D_M) is correlated with the particle size. The catalyst with a smaller Au size gives the highest D_M value. In this series of Au catalysts, Au/TiO_2 has a D_M value of 53% for having the smallest particle size (2.2 nm) while Au/ZnO has 21% for having the largest gold particle size, thus has the smallest dispersion among the synthesized catalysts. Naturally, Au/C (W) has an even lower dispersion (11%), given its higher Au nanoparticle size (10.5 nm).
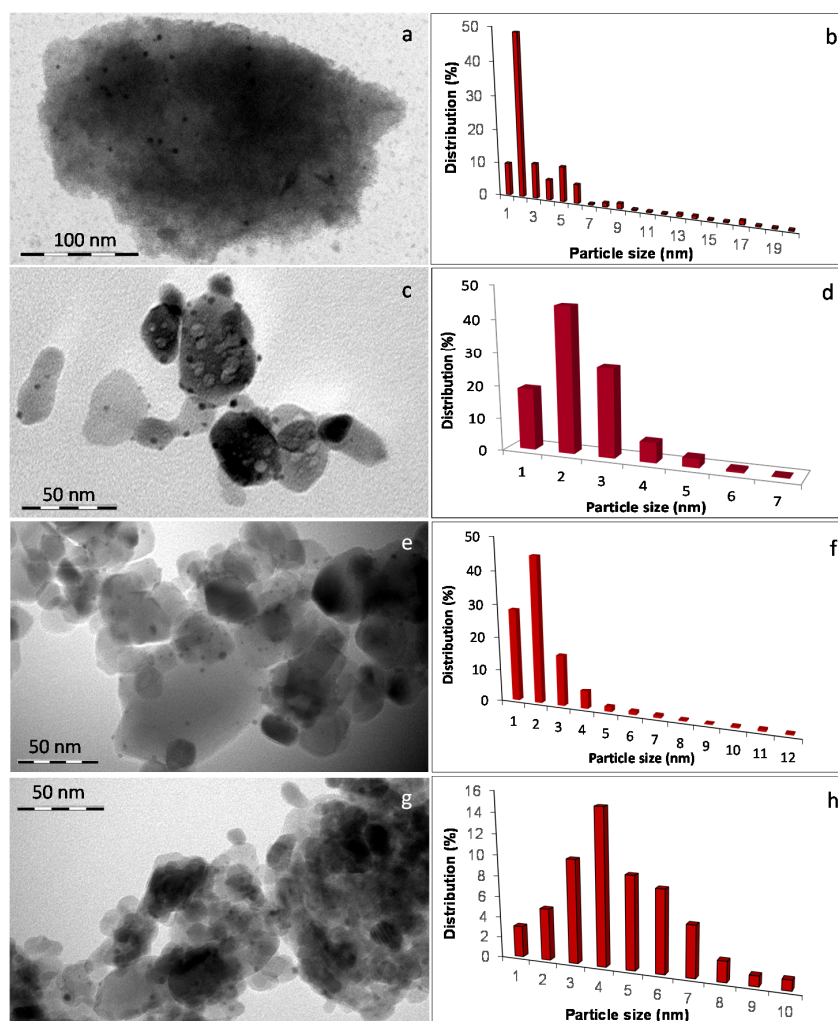
Figure 4. HRTEM images and their corresponding size distribution histograms of Au nanoparticles in (**a**,**b**) Au/Al$_2$O$_3$, (**c**,**d**) Au/Fe$_2$O$_3$, (**e**,**f**) Au/TiO$_2$, (**g**,**h**) Au/ZnO. Histograms adapted from [5] with permission from Wiley.

Table 2. Characterization of the supported Au materials [a].

Au Material	Au Material				
	Size Range, nm	Average Particle Size, nm	Oxidation State	Loading, wt%	Dispersion,% [c]
Au/Al$_2$O$_3$	1–20	3.6	Au^0	0.7	32
Au/Fe$_2$O$_3$	1–7	2.3	Au$^+$	0.8	50
Au/TiO$_2$	1–12	2.2	Au$^+$	1.6	53
Au/ TiO$_2$ (W)	n.a.	3.7 [b]	n.a.	1.5	31
Au/ZnO	1–10	5.5	Au^0	1.2	21
Au/C (W)	n.a.	10.5 [b]	n.a.	1.0	11

[a] Data from [5], size range and particle size determined by TEM, oxidation state by XPS and Au loading determined by AAS. [b] Data from [40]. [c] Data from [56], except WGC catalysts. n.a.—not available.

2.2. Synthesis of 1,2,3-Triazoles Using Au NPs on Different Supports

On the outset of this investigation, the three-component one-pot reaction of benzyl bromide, sodium azide and phenylacetylene were initiated, as model substrates, for the optimization studies. The Au nanoparticles supported on Al$_2$O$_3$, Fe$_2$O$_3$, TiO$_2$ and ZnO, as well as the reference catalysts (viz., Au/TiO$_2$ {W} and Au/C {W}) were tested for

the microwave-assisted synthesis of 1,2,3-triazoles in a 1:1 mixture of water and acetonitrile (Scheme 1). The effect of temperature, catalyst loading and the volume of solvent were the investigated factors that could influence the catalytic activity. The results of the optimizations are listed in Table S1 and selected ones are shown in Table 3. Scheme 2 shows the synthesis of 1-benzyl-4-phenyl-1*H*-1,2,3-triazole.

Table 3. Selected data for the microwave-assisted synthesis of 1-benzyl-4-phenyl-1*H*-1,2,3-triazole catalyzed by Au nanoparticles on different metal oxide supports [a].

Entry	Catalyst	Catalyst Loading, [b] mol%	Temperature °C	Yield [c] %	TON [d]
1	Au/ZnO	0.1	100	28	279
2	Au/Fe$_2$O$_3$	0.1	100	41	414
3	Au/TiO$_2$	0.1	100	40	395
4	Au/Al$_2$O$_3$	0.1	100	43	431
5	Au/TiO$_2$ (W)	0.1	100	28	291
6	Au/C (W)	0.1	100	27	269
7	Au/ZnO	0.1	150	63	633
8	Au/Fe$_2$O$_3$	0.1	150	66	659
9	Au/TiO$_2$	0.1	150	64	639
10	Au/Al$_2$O$_3$	0.1	150	67	672
11	Au/TiO$_2$ (W)	0.1	150	60	602
12	Au/C (W)	0.1	150	62	622
13	Blank	-	150	28	n/a
14	Au/ZnO	0.5	150	67	134
15	Au/Fe$_2$O$_3$	0.5	150	73	146
16	Au/TiO$_2$	0.5	150	75	150
17	Au/Al$_2$O$_3$	0.5	150	70	140
18	Au/TiO$_2$ (W)	0.5	150	69	139
19	Au/C (W)	0.5	150	67	134
20	Au/TiO$_2$	1.0	150	79	79
21	Au/TiO$_2$	1.5	150	76	51
22	Au/TiO$_2$ [e]	0.5	150	74	149
23	Au/TiO$_2$ [f]	0.5	150	73	146

[a] Reaction conditions: benzyl bromide (0.30 mmol), phenylacetylene (0.33 mmol), NaN$_3$ (0.33 mmol), H$_2$O: MeCN (0.5 mL, 1:1 *v/v*), MW (30 W), 15 min. [b] Calculated vs. benzyl bromide. [c] Isolated yield. [d] Turnover number = moles of product per mol of catalyst. [e] NH$_4$OH (0.66 mmol) was added to the reaction mixture. [f] Trifluoroacetic acid (0.66 mmol) was added to the reaction mixture.
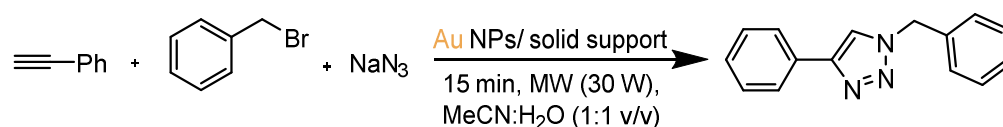
Scheme 2. Synthesis of 1-benzyl-4-phenyl-1*H*-1,2,3-triazole.

For the first two sets of experimental runs (Table 3, entries 1–12), the activity of the Au catalysts were probed at 100 °C and 150 °C using 0.1 mol% of the Au catalyst loading. The yields obtained at 100 °C (Table 3, entries 1–6) from the six Au catalysts varied from 27 to 43%. Increasing the temperature to 150 °C improved the yield to at least 60% (TON = 600–670) (Table 3, entries 7–12). A blank reaction was also performed under the same conditions and gave a mixture of 1,4- and 1,5-triazoles in a ~50:50 ratio as shown in the ^{1}H NMR spectrum (Supplementary Figure S3) with a total yield of 28% (Table 3, entry 13). At 150 °C, increasing the catalyst loading from 0.1 to 0.5 mol% slightly improved the reaction yield (Table 3, compare entries 7–12 and 14–19) with the catalyst Au/TiO$_2$ being the most active one in terms of the high obtained yield (Table 3, entry 16). The high catalytic activity of Au/TiO$_2$ might be correlated to the particle size effect as it has the smallest particle size among the studied Au catalysts (Table 2). Two more reactions were performed using Au/TiO$_2$ with higher catalyst loadings of 1 and 1.5 mol% (Table 3,
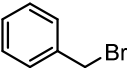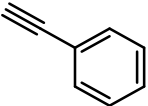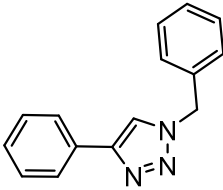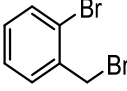
entries 20 and 21). In general, increasing the catalyst loading from 0.1 to 1 mol% improved the reaction yield from 64 to 79% (TON = 639, 150 and 79) (Table 3, entries 9, 16, 20), respectively, and a further increase of the catalyst amount to 1.5 mol% led to a slightly diminished yield of 76% (TON = 51) (Table 3, entry 21). This drop in yield could be attributed to the formation of Au-agglomerates with high catalyst loadings, which would decrease the active metal sites dispersion and the catalyst efficacy. Addition of NH_4OH or trifluoroacetic acid, as additives, (Table 3, entries 22 and 23) were also explored to determine if an increase in the yield would be observed. However, the isolated yields (73%, TON = 146 and 74%, TON = 149) were almost the same as the one without additives. Tests for the metal oxide supports were also performed and the yields were obtained only in the 27–31% range (Supplementary Table S1, entries 49–52). This indicates that the presence of Au particles led to an increased activity compared with the supports alone. The ^1H NMR spectra of the product obtained in the reaction catalyzed by the supports (Supplementary Figures S13–S16) show regioselectivity towards the 1,4-triazole product, but a few impurities assigned to the 1,5-triazole peaks were also observed.

Comparing the catalytic activity of the catalyst Au/TiO_2 (Table 3, entry 16) to the reference catalyst Au/TiO_2 (W) (Table 3, entry 18) shows once again the effect of the particle size on the activity of the catalyst as Au/TiO_2, which has a lower average particle diameter of gold (Table 2), is more active than Au/TiO_2 (W) using the same metal loading. Catalysts Au/ZnO and Au/C, in most cases, gave lower yields when compared to others due to their larger gold nanoparticle sizes (Table 2). Smaller particles typically exhibited better catalytic activity, but the characteristics of the support and its interaction with Au could also contribute [5,57]. Also, 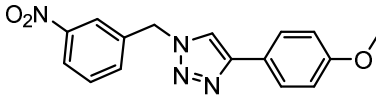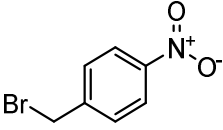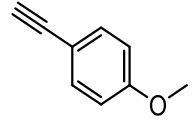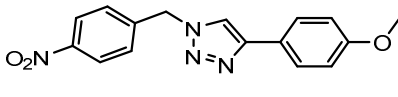there is no direct evidence that the Au-dispersion and particle size will depend on the textural properties of supports alone, as they are dependent also on several factors, such as, metal loading and the pretreatment conditions.

It is worth noting that the catalysts that present the highest yields (Au/TiO_2 and Au/Fe_2O_3) show the same gold oxidation state (Au^+), smaller gold particle sizes (2.2 and 2.3 nm, respectively), and consequently the highest dispersions of gold nanoparticles (53 and 50%, respectively). However, the catalytic performance of Au/Al_2O_3 is also comparable to those of Au/TiO_2 and Au/Fe_2O_3 despite the intermediate nanoparticle size (3.6 nm) and reduced oxidation state (Au^0). This comparable catalytic activity could be attributed to the higher BET surface area (210 $m^2 g^{-1}$), pore volume –(1.24 $cm^3 g^{-1}$) and pore size (19.6 nm). On the other hand, the low performance of Au/ZnO among the prepared catalysts, besides having the largest particle size (5.5 nm), small BET surface area (25 $m^2 g^{-1}$), pore volume (0.08 $cm^3 g^{-1}$) and reduced oxidation state of Au (Au^0), is most likely due to the effect of oxygen vacancies in ZnO at Au/ZnO interface. Based on related literature, the varying degree of oxygen deficiencies are of fundamental importance for explaining the catalytic activity of Au/ZnO [58–60]. The O 1s XPS spectrum of ZnO (see Supporting Materials, Figure S18) shows two deconvoluted peaks. The peak at ~532.4 eV can be correlated with O^{2-} in the oxygen-deficient regions (O_{II}), which could reflect the concentration of oxygen vacancies [61] and the peak at low BE near 530.8 eV is assigned to the surface lattice oxygen species (O_I) [62]. As reported, the relative amounts of O_{II} among the catalysts is in the order: Au/ZnO > Au/Fe_2O_3 > Au/TiO_2 > Au/Al_2O_3 (Supplementary Figure S18) [5], indicating that the ZnO support contains high oxygen-vacancy concentrations It has been reported previously that the presence of low oxygen-vacancy concentrations in ZnO support results in an increase in the work function of ZnO, which facilitates electron transfer and makes the formation of the Au/ZnO interface thermodynamically more favorable [58]. Since the opposite is true for our sample, as a consequence, Au/ZnO has low catalytic activity.

To evaluate the scope of the supported gold nanoparticle-catalyzed AAC reaction, several substituted benzyl bromide and terminal alkyne substrates were used to obtain the corresponding 1,4-disubstituted-1,2,3-triazoles (Table 4). The optimized conditions using Au/TiO_2 (Table 3, entry 20) were employed. The reaction is shown in Scheme 3. In all cases, the 1,4-disubstituted-1,2,3-triazoles were selectively obtained with good yields up to 79%.

Table 4. Cycloaddition reaction of azides and alkynes catalyzed by Au/TiO$_2$ [a].

Entry	Benzyl Bromide	Alkyne	Product	Yield, [b] %	TON, [c]
1				79	79
2				62	62
3				74	74
4				71	71
5				75	75
6				46	46
7				39	39
8				71	71
9				63	63
10				64	64
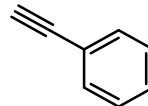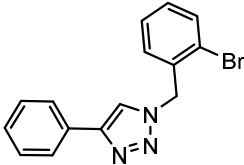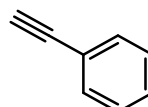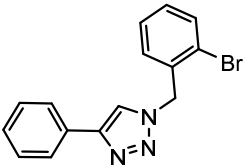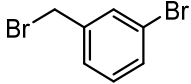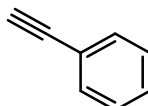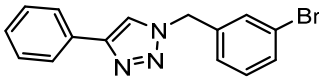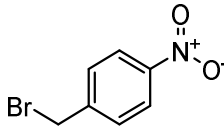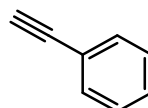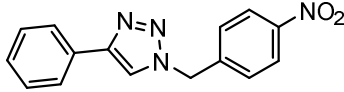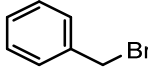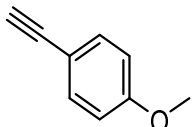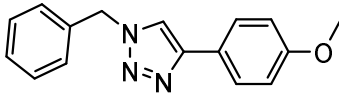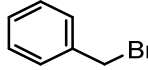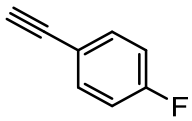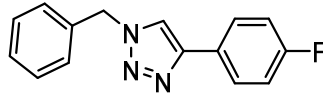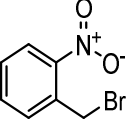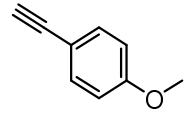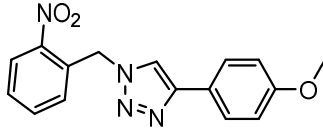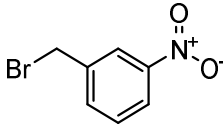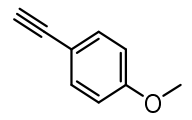
[a] Reaction conditions: benzyl bromide (0.30 mmol), phenylacetylene (0.33 mmol), NaN$_3$ (0.33 mmol), H$_2$O: MeCN (0.5 mL, 1:1 *v/v*), MW (30 W, 150 °C), 15 min, 1.0 mol% of Au catalysts vs. benzyl bromide derivatives. [b] Isolated yield. [c] Turnover number = moles of product per mol of catalyst.
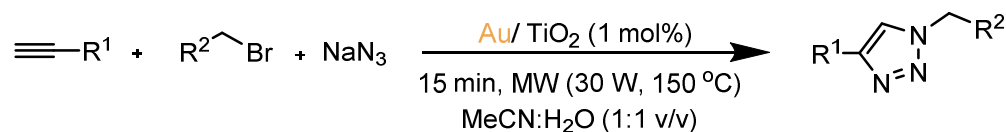
Scheme 3. Synthesis of triazoles catalyzed by Au/TiO$_2$ under MW irradiation.

Studies of Au NPs as potential catalysts for click reactions is limited to a very few reports. Muthusubramanian et al. [4] used nanoporous titania-supported Au NPs as catalysts for the AAC reaction to obtain triazoles with good to excellent yields up to 97% in 45 min at 60 °C. Huang et al. [18] also evaluated the ability of unsupported polyhedral gold nanocrystals in the catalysis of AAC and the triazole products were obtained in good yields up to 72% after 6 h. The previously studied protocols for AuAAC were able to obtain triazoles in good to excellent yields, but the methodologies used involved conventional heating for longer reaction times and sequential mode of reaction using the unfavorable organic azides. The present method for AuAAC is more advantageous in terms of the regioselective synthesis of 1,4-disubstituted-1,2,3-triazoles in good yields up to 79% using lower catalyst loading of 0.5–1.0 mol in a shorter time frame of 15 min via a three components one-pot, microwave-assisted method without using organic azides, which were obtained in situ by the reaction of benzyl bromide and sodium azide.

In analogy with previous reports [4,18,63], a conceivable mechanism of the Au-AAC reaction is depicted in Scheme 4. The proposed mechanism involves the reduction of the electron density with increase of acidity of the 1-alkyne upon coordination to a gold atom, resulting in the liberation of the terminal hydrogen as a proton, with formation of an alkynyl (acetylide) species (R^1−C≡C−Au). Hence, gold is behaving as a carbophilic Lewis acid, as expected [16]. A nucleophilic attack of the organoazide to the unsaturated CC bond occurs subsequently, at the C2-carbon of R^1-C≡C-Au or of a related digold species where the unsaturated CC bond is further activated by a second Au atom, as proposed in the Scheme (step 2). This overall step involves the coordination of the organoazide via the nitrogen proximal to carbon [4] and the nucleophilic attack at the alkynyl C-2 carbon by the distal nitrogen of the azide forming a six-membered intermediate via an oxidative addition to a gold metal [64]. A reductive ring contraction then follows to afford the triazolide intermediate (step 3), which undergoes a fast protonation (step 4) to release the 1,2,3-triazole as product and regenerate the gold catalyst for the next cycle [65].

The recyclability of the catalyst Au/TiO$_2$ was probed using the reaction conditions described in Table 3, entry 20, for five consecutive cycles (Figure 5). After each run, the catalyst was separated from the reaction mixture, washed thoroughly with distilled water, and dried overnight before using in the next run. As shown in Figure 5, the yield values decreased after each successive cycle. After the fifth cycle, the reused catalyst was analyzed with TEM (Supplementary Figure S17) and ICP-AES (inductively coupled plasma—atomic emission spectroscopy). As not much Au particles were seen on the used catalyst, it was not possible to obtain a particle size distribution with accuracy. However, it can be observed that the size of the Au nanoparticles increased up to 30 nm (after fifth cycle) due to agglomeration. The ICP-AES result also revealed a decrease in the amount of% Au in the catalyst, from 1.6% to 0.26%. These factors explain the observed drop in the catalytic activity of Au/TiO$_2$ after five successive cycles.
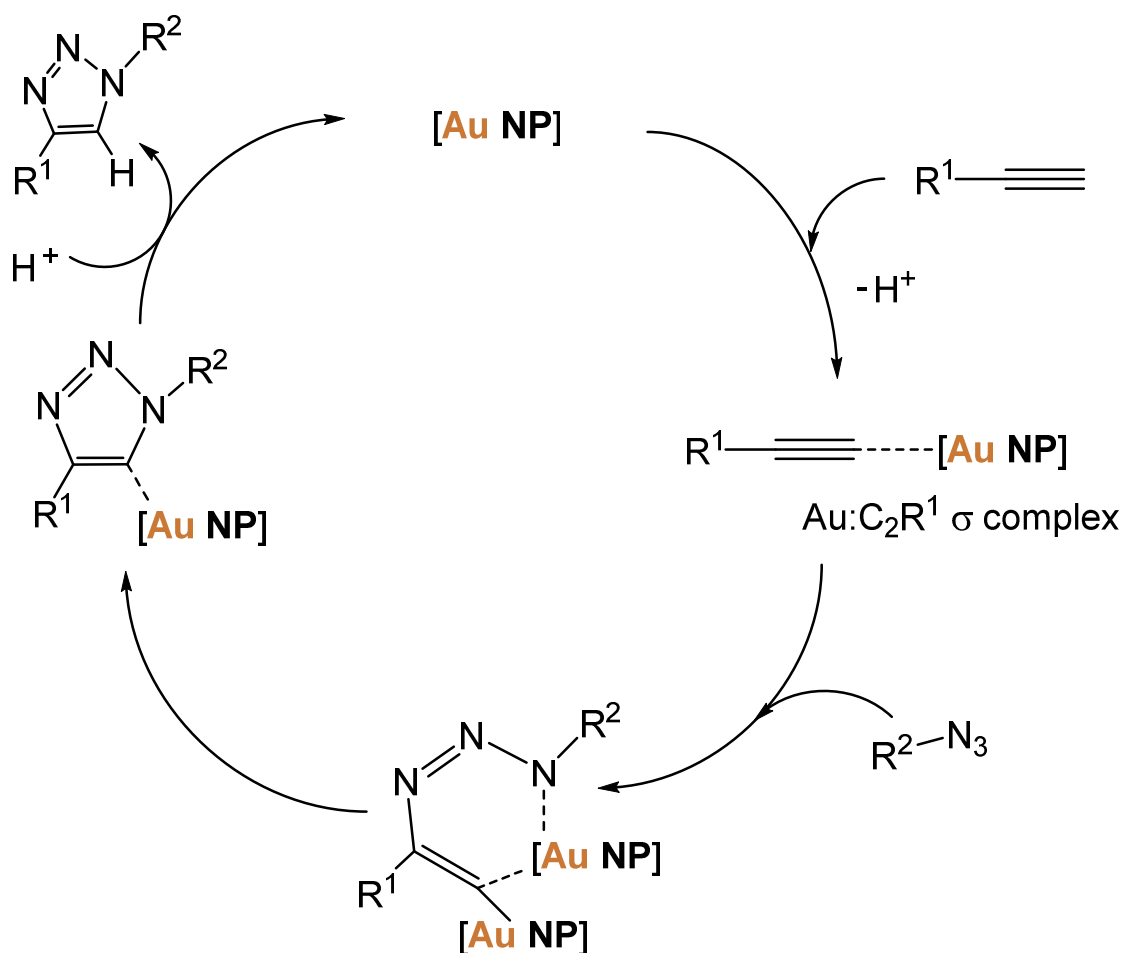
Scheme 4. Proposed mechanism for the AuAAC reaction.
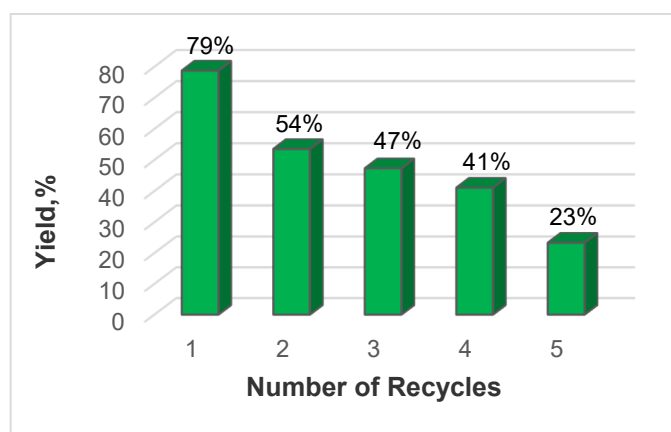
Figure 5. Effect of Au/TiO$_2$ recycling on the yield of 1,2,3-triazole product. Reaction conditions: 1.0 mol% of Au/TiO$_2$ vs. benzyl bromide, 15 min, MW (30 W, 150 °C).

3. Experimental

3.1. Materials

Reagents and solvents were obtained from commercial sources and used without further purification. Reference catalysts, 1.5% Au/TiO$_2$ (Type A) and 1% Au/C (Type D), were purchased from the World Gold Council (WGC, London, UK). The gold sample HAuCl$_4 \cdot 3$ H$_2$O was from Alfa Aesar (Kandel, Germany). Four different types of oxides were used

as received: Al_2O_3 (<50 nm) from Aldrich (Darmstadt, Germany), Fe_2O_3 (powder) from Sigma Aldrich, TiO_2 (P25) from Evonik Degussa (Essen, Germany) and ZnO (AdNano VP 20) from Evonik Degussa. ^{1}H-, ^{13}C- and DEPT NMR spectra were obtained using an Avance II 300 MHz NMR spectrometer (Bruker, Billerica, MA, USA) at ambient temperature. The chemical shifts were reported in ppm using tetramethylsilane as an internal reference. A Monowave 300 microwave reactor (Anton Paar GmbH, Graz, Austria) was used for this study.

3.2. Deposition of Au NPs

Gold (~1 wt%) supported on different solid supports (Al_2O_3, Fe_2O_3, TiO_2, and ZnO) was prepared by deposition-precipitation method [5]. A 1M NaOH solution was added to $HAuCl_4$ (5×10^{-3} M) to have a final pH = 9. The solid support was subsequently added (1 g per 50 mL of solution) while stirring the slurry at room temperature for 1 h. The suspension was then filtered, and the residue was thoroughly washed with distilled water and oven-dried at 110 °C overnight. Gold reference catalysts, supplied by the World Gold Council (W) [40] were also used for comparison, namely gold on carbon black, Au/C Gold Catalyst (Type D, 1% Au) and gold on titania, Au/TiO_2 (Type A, 1.5% Au).

3.3. Characterization of the Supported Au Nanoparticles

In order to determine the Au loading, the samples were pre-treated with aqua regia for 2 h and then subjected to atomic absorption spectroscopy (AAS) using a UNICAM spectrophotometer (Algés, Portugal). For HRTEM studies, a CM-20 electron microscope located at Granada University (Phillips, Amsterdam, Netherlands) was used while EDS confirmed the existence of Au on the supports. Magnification was 600,000× with maximum resolution of 0.27 nm between points and 0.14 nm between lines. For the analysis, the samples were prepared by dispersion of the solid catalyst in isopropyl alcohol followed by suspension deposition onto a carbon film located on a copper grid. Nanoparticle sizes were measure from HR-TEM images using the ImageJ program. The average particle size was measured based on the sizes of ~300–500 particles, depending on the sample being analyzed. The average NP sizes were calculated for all samples.

The dispersion (D_M) of Au particles is defined as the ratio between the number of surface metal atoms to the total number of metal atoms and was calculated by $D_M = (6Mn_s)/(\varrho Nd_p)$, where n_s = number of atoms at the surface per unit area (1.15×10^{19} m^{-2} for Au), M = molar mass of Au (196.97 g mol^{-1}), ϱ = density of Au (19.5 g cm^{-3}), N = Avogadro's number (6.022×10^{23} mol^{-1}), and d_p = average particle size (nm) (from HRTEM, assuming the Au particles are spherical) [53,56,66]. In textural studies, N_2 adsorption isotherms (−196 °C, a Quantachrome Nova 4200e instrument) were obtained for samples pretreated in vacuum. The multi-point Brunnauer-Emmet-Teller (BET) method was used to determine their specific surface area. Pore size distributions were obtained using the BJH (Barrett-Joyner-Halenda) desorption method. The total pore volume was calculated at $P/P_o = 0.99$. Morphological characterization was performed by SEM using a Quanta 400 FEG ESEM (15 keV) electron microscope (FEI, Lausanne, Switzerland).

XPS analysis was determined by an ESCALAB 200A spectrometer (VG Scientific, Whaltham, MA, USA) using AlKα radiation source (1486.6 eV). All spectra were calibrated relative to a C 1s peak positioned at 285 eV for charge shifts correction and CASA XPS program was employed to fit experimental curves in a non-linear least square fitting routine.

H_2-TPR experiments were carried out on the oxides using the AMI-200 Catalyst Characterisation Instrument (Altamira Instruments, Pittsburgh, PA, USA) where the sample (50 mg) was placed in a flow installation (1100 °C at 10 °C/min under He flow of 29 mL/min and H_2 flow of 1.5 mL/min).

XRD analysis was carried out in an X'Pert MPD (PAN'alytical, Malvern, UK) equipped with a X'Celerator detector and secondary monochromator (Cu Kα λ = 0.154 nm, 50 kV, 40 mA; data recorded at 0.017° step size, 100 s/step). Rietveld refinement using PowderCell

software was used to identify the existing crystallographic phases. Further details can be found in the previous works [53–55].

3.4. Gold Nanoparticle-Catalyzed Azide-Alkyne Cycloaddition Reaction

To a 10 mL borosilicate glass vial, equipped with a magnetic stir bar, was added a mixture of benzyl bromide (0.30 mmol), NaN_3 (0.33 mmol, 0.0215 g), phenylacetylene (0.33 mmol), supported Au catalyst (1.0 mol% relative to benzyl bromide) and 0.5 mL of solvent (H_2O:MeCN, 1:1 v/v). The reaction vial was tightly capped, placed in a microwave reactor, stirred (600 rpm) and simultaneously irradiated (30 W) for 15 min at 150 °C. During those experimental runs, the pressure was 5–6 bar. After the reaction, the mixture was cooled at room temperature and extracted with ethyl acetate to obtain the crude product through solvent evaporation. The yellowish solid was then washed with diethyl ether to give the off-white crystalline product with no further chromatographic isolation step required. The supported Au catalyst was separated by filtration and washed with water and dried to be reused as suitable.

4. Conclusions

The catalytic activity of Au NPs deposited on different solid supports (Al_2O_3, Fe_2O_3, TiO_2 and ZnO) in the microwave-assisted AuAAC reaction was investigated. All catalysts are active for this reaction and afford regioselectivity in the formation of the desired 1,4-disubstituted-1,2,3-trizoles, with Au/TiO_2 (presenting the lowest NP size) being the most active one in terms of the highest obtained yield. In the presence of catalyst Au/TiO_2, the one-pot three-component (alkyne, organohalide and sodium azide) AuAAC reactions were performed using several substrates to afford the corresponding triazoles in moderate yields up to 79% after 15 min, in a mixture of water and acetonitrile under MW (30 W, 150 °C) using 1 mol% of catalyst loading. The catalyst was recovered and reused up to five consecutive cycles although with loss of activity due to the increase of gold nanoparticle size.

In view of advantages, the current method displays several merits, including the utilization of inexpensive and readily available materials, mild reaction conditions, easy operation and the recyclability of the catalyst. The combination of remarkable features of AuAAC in a one-pot system paves the way for subsequent applications in various contexts, thereby complementing the well-known copper- and ruthenium-based catalytic AAC systems. It also offers a breadth of interest to those working in triazole-related modifications and their corresponding material advancements.

Conflicts of Interest: The authors declare no conflict of interest.

References

1. Chng, L.L.; Erathodiyil, N.; Ying, J.Y. Nanostructured catalysts for organic transformations. *Acc. Chem. Res.* **2013**, *46*, 1825–1837. [CrossRef]
2. Wang, D.; Li, Y. Bimetallic nanocrystals: Liquid-phase synthesis and catalytic applications. *Adv. Mater.* **2011**, *23*, 1044–1060. [CrossRef]
3. Polshettiwar, V.; Len, C.; Fihri, A. Silica-supported palladium: Sustainable catalysts for cross-coupling reactions. *Coord. Chem. Rev.* **2009**, *253*, 2599–2626. [CrossRef]
4. Boominathan, M.; Pugazhenthiran, N.; Nagaraj, M.; Muthusubramanian, S.; Murugesan, S.; Bhuvanesh, N. Nanoporous titania-supported gold nanoparticle-catalyzed green synthesis of 1,2,3-triazoles in aqueous medium. *ACS Sustain. Chem. Eng.* **2013**, *1*, 1405–1411. [CrossRef]
5. Martins, L.M.D.R.S.; Carabineiro, S.A.C.; Wang, J.; Rocha, B.G.M.; Maldonado-Hódar, F.J.; Pombeiro, A.J.L.O. Supported Gold Nanoparticles as Reusable Catalysts for Oxidation Reactions of Industrial Significance. *ChemCatChem* **2017**, *9*, 1211–1221. [CrossRef]
6. Polshettiwar, V.; Varma, R.S. Green chemistry by nano-catalysis. *Green Chem.* **2010**, *12*, 743–775. [CrossRef]
7. Yan, N.; Xiao, C.; Kou, Y. Transition metal nanoparticle catalysis in green solvents. *Coord. Chem. Rev.* **2010**, *254*, 1179–1218. [CrossRef]
8. deAlmeida, M.P.; Carabineiro, S.A.C. The Best of Two Worlds from the Gold Catalysis Universe: Making Homogeneous Heterogeneous. *ChemCatChem* **2012**, *4*, 18–29. [CrossRef]
9. Hashmi, A.S.K. Homogeneous catalysis by gold. *Gold Bull.* **2004**, *37*, 51–65. [CrossRef]
10. Zhou, J.; Ralston, J.; Sedev, R.; Beattie, D.A. Functionalized gold nanoparticles: Synthesis, structure and colloid stability. *J. Colloid Interface Sci.* **2009**, *331*, 251–262. [CrossRef]
11. Hughes, M.D.; Xu, Y.J.; Jenkins, P.; McMorn, P.; Landon, P.; Enache, D.I.; Carley, A.F.; Attard, G.A.; Hutchings, G.J.; King, F.; et al. Tunable gold catalysts for selective hydrocarbon oxidation under mild conditions. *Nature* **2005**, *437*, 1132–1135. [CrossRef]
12. Turner, M.; Golovko, V.B.; Vaughan, O.P.H.; Abdulkin, P.; Berenguer-Murcia, A.; Tikhov, M.S.; Johnson, B.F.G.; Lambert, R.M. Selective oxidation with dioxygen by gold nanoparticle catalysts derived from 55-atom clusters. *Nature* **2008**, *454*, 981–983. [CrossRef] [PubMed]
13. Bujak, P.; Bartczak, P.; Polanski, J. Highly efficient room-temperature oxidation of cyclohexene and d-glucose over nanogold Au/SiO$_2$ in water. *J. Catal.* **2012**, *295*, 15–21. [CrossRef]
14. Jin, Z.; Song, Y.Y.; Fu, X.P.; Song, Q.S.; Jia, C.J. Nanoceria Supported Gold Catalysts for CO Oxidation. *Chin. J. Chem.* **2018**, *36*, 639–643. [CrossRef]
15. Carrettin, S.; Blanco, M.C.; Corma, A.; Hashmi, A.S.K. Heterogeneous gold-catalysed synthesis of phenols. *Adv. Synth. Catal.* **2006**, *348*, 1283–1288. [CrossRef]
16. Corma, A.; Leyva-Pérez, A.; Sabater, M.J. Gold-Catalyzed Carbon–Heteroatom Bond-Forming Reactions. *Chem. Rev.* **2011**, *111*, 1657–1712. [CrossRef]
17. Stephen, A.; Hashmi, K. Homogeneous gold catalysis beyond assumptions and proposals-characterized intermediates. *Angew. Chem. Int. Ed.* **2010**, *49*, 5232–5241. [CrossRef]
18. Rej, S.; Chanda, K.; Chiu, C.-Y.; Huang, M.H. Control of Regioselectivity over Gold Nanocrystals of Different Surfaces for the Synthesis of 1,4-Disubstituted Triazole through the Click Reaction. *Chem.-Eur. J.* **2014**, *20*, 15991–15997. [CrossRef]
19. Díaz Arado, O.; Mönig, H.; Wagner, H.; Franke, J.H.; Langewisch, G.; Held, P.A.; Studer, A.; Fuchs, H. On-surface azide-alkyne cycloaddition on Au(111). *ACS Nano* **2013**, *7*, 8509–8515. [CrossRef] [PubMed]
20. Agalave, S.G.; Maujan, S.R.; Pore, V.S. Click chemistry: 1,2,3-triazoles as pharmacophores. *Chem.-Asian J.* **2011**, *6*, 2696–2718. [CrossRef] [PubMed]
21. Tullis, J.S.; VanRens, J.C.; Natchus, M.G.; Clark, M.P.; De, B.; Hsieh, L.C.; Janusz, M.J. The development of new triazole based inhibitors of tumor necrosis factor-α (TNF-α) production. *Bioorg. Med. Chem. Lett.* **2003**, *13*, 1665–1668. [CrossRef]
22. Chu, C.; Liu, R. Application of click chemistry on preparation of separation materials for liquid chromatography. *Chem. Soc. Rev.* **2011**, *40*, 2177–2188. [CrossRef]

23. Lau, Y.H.; Rutledge, P.J.; Watkinson, M.; Todd, M.H. Chemical sensors that incorporate click-derived triazoles. *Chem. Soc. Rev.* **2011**, *40*, 2848–2866. [CrossRef]

24. Mahmoud, A.G.; Guedes Da Silva, M.F.C.; Sokolnicki, J.; Smoleński, P.; Pombeiro, A.J.L. Hydrosoluble Cu(I)-DAPTA complexes: Synthesis, characterization, luminescence thermochromism and catalytic activity for microwave-assisted three-component azide-alkyne cycloaddition click reaction. *Dalt. Trans.* **2018**, *47*, 7290–7299. [CrossRef] [PubMed]

25. Mahmoud, A.G.; Martins, L.M.D.R.S.; Guedes da Silva, M.F.C.; Pombeiro, A.J.L. Copper complexes bearing C-scorpionate ligands: Synthesis, characterization and catalytic activity for azide-alkyne cycloaddition in aqueous medium. *Inorg. Chim. Acta* **2018**, *483*, 371–378. [CrossRef]

26. Mahmoud, A.G.; Guedes Da Silva, M.F.C.; Mahmudov, K.T.; Pombeiro, A.J.L. Arylhydrazone ligands as Cu-protectors and -catalysis promoters in the azide-alkyne cycloaddition reaction. *Dalt. Trans.* **2019**, *48*, 1774–1785. [CrossRef]

27. Mahmoud, A.G.; Smolénski, P.; Guedes Da Silva, M.F.C.; Pombeiro, A.J.L. Water-Soluble O-, S-and Se-Functionalized Cyclic Acetyl-triaza-phosphines. Synthesis, Characterization and Application in Catalytic Azide-alkyne Cycloaddition. *Molecules* **2020**, *25*, 5479. [CrossRef]

28. Mahmoud, A.G.; Guedes da Silva, M.F.C.; Pombeiro, A.J.L. A new amido-phosphane as ligand for copper and silver complexes. Synthesis, characterization and catalytic application for azide–alkyne cycloaddition in glycerol. *Dalt. Trans.* **2021**, *50*, 6109–6125. [CrossRef] [PubMed]

29. Librando, I.L.; Mahmoud, A.G.; Carabineiro, S.A.C.; Guedes Da Silva, M.F.C.; Geraldes, C.F.G.C.; Pombeiro, A.J.L. The catalytic activity of carbon-supported Cu(I)-phosphine complexes for the microwave-assisted synthesis of 1,2,3-triazoles. *Catalysts* **2021**, *11*, 185. [CrossRef]

30. Librando, I.L.; Mahmoud, A.G.; Carabineiro, S.A.C.; Guedes da Silva, M.F.C.; Geraldes, C.F.G.C.; Pombeiro, A.J.L. Synthesis of a novel series of Cu(I) complexes bearing alkylated 1,3,5-triaza-7-phosphaadamantane as homogeneous and carbon-supported catalysts for the synthesis of 1-and 2-substituted-1,2,3-triazoles. *Nanomaterials* **2021**, *11*, 2702. [CrossRef] [PubMed]

31. Gomes, R.S.; Jardim, G.A.M.; de Carvalho, R.L.; Araujo, M.H.; da Silva Júnior, E.N. Beyond copper-catalyzed azide-alkyne 1,3-dipolar cycloaddition: Synthesis and mechanism insights. *Tetrahedron* **2019**, *75*, 3697–3712. [CrossRef]

32. Kalra, P.; Kaur, R.; Singh, G.; Singh, H.; Singh, G.; Pawan; Kaur, G.; Singh, J. Metals as "Click" catalysts for alkyne-azide cycloaddition reactions: An overview. *J. Organomet. Chem.* **2021**, *944*, 121846. [CrossRef]

33. Rostovtsev, V.V.; Green, L.G.; Fokin, V.V.; Sharpless, K.B. A stepwise huisgen cycloaddition process: Copper(I)-catalyzed regioselective "ligation" of azides and terminal alkynes. *Angew. Chem. Int. Ed.* **2002**, *41*, 2596–2599. [CrossRef]

34. Tornøe, C.W.; Christensen, C.; Meldal, M. Peptidotriazoles on solid phase: [1,2,3]-Triazoles by regiospecific copper(I)-catalyzed 1,3-dipolar cycloadditions of terminal alkynes to azides. *J. Org. Chem.* **2002**, *67*, 3057–3064. [CrossRef]

35. Speers, A.E.; Adam, G.C.; Cravatt, B.F. Activity-based protein profiling in vivo using a copper(I)-catalyzed azide-alkyne [3 + 2] cycloaddition. *J. Am. Chem. Soc.* **2003**, *125*, 4686–4687. [CrossRef] [PubMed]

36. Binder, W.; Kluger, C. Azide/Alkyne- "Click" Reactions: Applications in Material Science and Organic Synthesis. *Curr. Org. Chem.* **2006**, *10*, 1791–1815. [CrossRef]

37. Lutz, J.F. 1,3-Dipolar cycloadditions of azides and alkynes: A universal ligation tool in polymer and materials science. *Angew. Chem. Int. Ed.* **2007**, *46*, 1018–1025. [CrossRef] [PubMed]

38. Alonso, F.; Moglie, Y.; Radivoy, G.; Yus, M. Copper nanoparticles in click chemistry: An alternative catalytic system for the cycloaddition of terminal alkynes and azides. *Tetrahedron Lett.* **2009**, *50*, 2358–2362. [CrossRef]

39. Mularski, J.; Czaplińska, B.; Cieślik, W.; Bebłot, J.; Bartczak, P.; Sitko, R.; Polański, J.; Musiol, R. Electrolytic copper as cheap and effective catalyst for one-pot triazole synthesis. *Sci. Rep.* **2018**, *8*, 4496. [CrossRef] [PubMed]

40. World Gold Council. Available online: https://www.gold.org/news-and-events/press-releases/gold-reference-catalysts-now-available-international-standard (accessed on 25 June 2021).

41. Carabineiro, S.A.C.; Tavares, P.B.; Figueiredo, J.L. Gold on oxide-doped alumina supports as catalysts for CO oxidation. *Appl. Nanosci.* **2012**, *2*, 35–46. [CrossRef]

42. Milone, C.; Crisafulli, C.; Ingoglia, R.; Schipilliti, L.; Galvagno, S. A comparative study on the selective hydrogenation of α,β unsaturated aldehyde and ketone to unsaturated alcohols on Au supported catalysts. *Catal. Today* **2007**, *122*, 341–351. [CrossRef]

43. Albonetti, S.; Bonelli, R.; Delaigle, R.; Femoni, C.; Gaigneaux, E.M.; Morandi, V.; Ortolani, L.; Tiozzo, C.; Zacchini, S.; Trifirò, F. Catalytic combustion of toluene over cluster-derived gold/iron catalysts. *Appl. Catal. A Gen.* **2010**, *372*, 138–146. [CrossRef]

44. Solsona, B.E.; Garcia, T.; Jones, C.; Taylor, S.H.; Carley, A.F.; Hutchings, G.J. Supported gold catalysts for the total oxidation of alkanes and carbon monoxide. *Appl. Catal. A Gen.* **2006**, *312*, 67–76. [CrossRef]

45. Hua, J.; Wei, K.; Zheng, Q.; Lin, X. Influence of calcination temperature on the structure and catalytic performance of Au/iron oxide catalysts for water-gas shift reaction. *Appl. Catal. A Gen.* **2004**, *259*, 121–130. [CrossRef]

46. Neri, G.; Visco, A.M.; Galvagno, S.; Donato, A.; Panzalorto, M. Au/iron oxide catalysts: Temperature programmed reduction and X-ray diffraction characterization. *Thermochim. Acta* **1999**, *329*, 39–46. [CrossRef]

47. PalDey, S.; Gedevanishvili, S.; Zhang, W.; Rasouli, F. Evaluation of a spinel based pigment system as a CO oxidation catalyst. *Appl. Catal. B Environ.* **2005**, *56*, 241–250. [CrossRef]

48. Khoudiakov, M.; Gupta, M.C.; Deevi, S. Au/Fe$_2$O$_3$ nanocatalysts for CO oxidation: A comparative study of deposition-precipitation and coprecipitation techniques. *Appl. Catal. A Gen.* **2005**, *291*, 151–161. [CrossRef]

49. Zhang, C.; He, H.; Tanaka, K. ichi Catalytic performance and mechanism of a Pt/TiO$_2$ catalyst for the oxidation of formaldehyde at room temperature. *Appl. Catal. B Environ.* **2006**, *65*, 37–43. [CrossRef]

50. Wu, Y.; Sun, K.Q.; Yu, J.; Xu, B.Q. A key to the storage stability of Au/TiO$_2$ catalyst. *Phys. Chem. Chem. Phys.* **2008**, *10*, 6399–6404. [CrossRef] [PubMed]

51. Liang, M.; Kang, W.; Xie, K. Comparison of reduction behavior of Fe$_2$O$_3$, ZnO and ZnFe$_2$O$_4$ by TPR technique. *J. Nat. Gas Chem.* **2009**, *18*, 110–113. [CrossRef]

52. Valenzuela, M.A.; Bosch, P.; Jiménez-Becerrill, J.; Quiroz, O.; Páez, A.I. Preparation, characterization and photocatalytic activityof ZnO, Fe$_2$O$_3$ and ZnFe$_2$O$_4$. *J. Photochem. Photobiol. A Chem.* **2002**, *148*, 177–182. [CrossRef]

53. Carabineiro, S.A.C.; Machado, B.F.; Bacsa, R.R.; Serp, P.; Draić, G.; Faria, J.L.; Figueiredo, J.L. Catalytic performance of Au/ZnO nanocatalysts for CO oxidation. *J. Catal.* **2010**, *273*, 191–198. [CrossRef]

54. Carabineiro, S.A.C.; Bogdanchikova, N.; Tavares, P.B.; Figueiredo, J.L. Nanostructured iron oxide catalysts with gold for the oxidation of carbon monoxide. *RSC Adv.* **2012**, *2*, 2957–2965. [CrossRef]

55. Rodrigues, C.S.D.; Carabineiro, S.A.C.; Maldonado-Hódar, F.J.; Madeira, L.M. Wet peroxide oxidation of dye-containing wastewaters using nanosized Au supported on Al$_2$O$_3$. *Catal. Today* **2017**, *280*, 165–175. [CrossRef]

56. Rodrigues, C.S.D.; Carabineiro, S.A.C.; Maldonado-Hódar, F.J.; Madeira, L.M. Orange II Degradation by Wet Peroxide Oxidation Using Au Nanosized Catalysts: Effect of the Support. *Ind. Eng. Chem. Res.* **2017**, *56*, 1988–1998. [CrossRef]

57. Zhou, X.; Xu, W.; Liu, G.; Panda, D.; Chen, P. Size-dependent catalytic activity and dynamics of gold nanoparticles at the single-molecule level. *J. Am. Chem. Soc.* **2010**, *132*, 138–146. [CrossRef]

58. Wu, G.; Zhao, G.; Sun, J.; Cao, X.; He, Y.; Feng, J.; Li, D. The effect of oxygen vacancies in ZnO at an Au/ZnO interface on its catalytic selective oxidation of glycerol. *J. Catal.* **2019**, *377*, 271–282. [CrossRef]

59. Strunk, J.; Kähler, K.; Xia, X.; Comotti, M.; Schüth, F.; Reinecke, T.; Muhler, M. Au/ZnO as catalyst for methanol synthesis: The role of oxygen vacancies. *Appl. Catal. A Gen.* **2009**, *359*, 121–128. [CrossRef]

60. Polarz, S.; Strunk, J.; Ischenko, V.; Van Den Berg, M.W.E.; Hinrichsen, O.; Muhler, M.; Driess, M. On the role of oxygen defects in the catalytic performance of zinc oxide. *Angew. Chem. Int. Ed.* **2006**, *45*, 2965–2969. [CrossRef]

61. Park, S.M.; Ikegami, T.; Ebihara, K. Effects of substrate temperature on the properties of Ga-doped ZnO by pulsed laser deposition. *Thin Solid Films* **2006**, *513*, 90–94. [CrossRef]

62. Chen, M.; Wang, X.; Yu, Y.H.; Pei, Z.L.; Bai, X.D.; Sun, C.; Huang, R.F.; Wen, L.S. X-ray photoelectron spectroscopy and auger electron spectroscopy studies of Al-doped ZO films. *Appl. Surf. Sci.* **2000**, *158*, 134–140. [CrossRef]

63. Kidwai, M.; Bansal, V.; Kumar, A.; Mozumdar, S. The first Au-nanoparticles catalyzed green synthesis of propargylamines via a three-component coupling reaction of aldehyde, alkyne and amine. *Green Chem.* **2007**, *9*, 742–774. [CrossRef]

64. Berg, R.; Straub, B.F. Advancements in the mechanistic understanding of the copper-catalyzed azide-alkyne cycloaddition. *Beilstein J. Org. Chem.* **2013**, *9*, 2715–2750. [CrossRef]

65. Maity, P.; Takano, S.; Yamazoe, S.; Wakabayashi, T.; Tsukuda, T. Binding motif of terminal alkynes on gold clusters. *J. Am. Chem. Soc.* **2013**, *135*, 9450–9457. [CrossRef] [PubMed]

66. Santos, V.P.; Carabineiro, S.A.C.; Bakker, J.J.W.; Soares, O.S.G.P.; Chen, X.; Pereira, M.F.R.; Órfão, J.J.M.; Figueiredo, J.L.; Gascon, J.; Kapteijn, F. Stabilized gold on cerium-modified cryptomelane: Highly active in low-temperature CO oxidation. *J. Catal.* **2014**, *309*, 58–65. [CrossRef]